Volume 140 | Number 23 | 7 December 2015 | Pages 7831–8058

Analyst

www.rsc.org/analyst

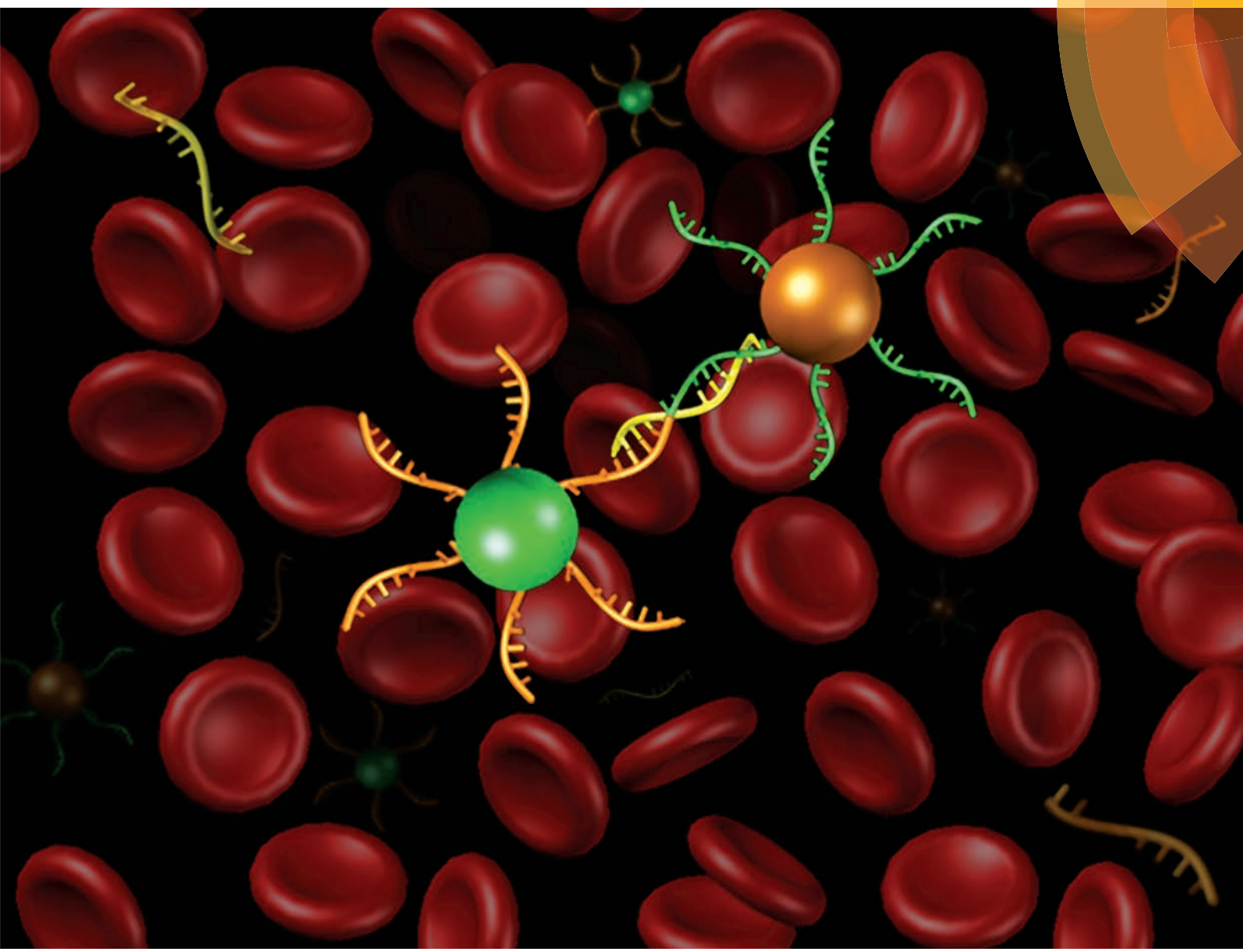

ISSN 0003-2654

ROYAL SOCIETY OF CHEMISTRY

PAPER
Ting-Hsuan Chen *et al.*
Visual detection of nucleic acids based on Mie scattering and the magnetophoretic effect

Analyst

PAPER

View Article Online
View Journal | View Issue

Cite this: *Analyst*, 2015, **140**, 7876

Visual detection of nucleic acids based on Mie scattering and the magnetophoretic effect†

Zichen Zhao,[a] Shan Chen,[a] John Kin Lim Ho,[a] Ching-Chang Chieng[a] and Ting-Hsuan Chen*[a,b,c]

Received 4th June 2015,
Accepted 19th August 2015

DOI: 10.1039/c5an01123j

www.rsc.org/analyst

Visual detection of nucleic acid biomarkers is a simple and convenient approach to point-of-care applications. However, issues of sensitivity and the handling of complex bio-fluids have posed challenges. Here we report on a visual method detecting nucleic acids using Mie scattering of polystyrene microparticles and the magnetophoretic effect. Magnetic microparticles (MMPs) and polystyrene microparticles (PMPs) were surface-functionalised with oligonucleotide probes, which can hybridise with target oligonucleotides in juxtaposition and lead to the formation of MMPs–targets–PMPs sandwich structures. Using an externally applied magnetic field, the magnetophoretic effect attracts the sandwich structure to the sidewall, which reduces the suspended PMPs and leads to a change in the light transmission *via* the Mie scattering. Based on the high extinction coefficient of the Mie scattering (~3 orders of magnitude greater than that of the commonly used gold nanoparticles), our results showed the limit of detection to be 4 pM using a UV-Vis spectrometer or 10 pM by direct visual inspection. Meanwhile, we also demonstrated that this method is compatible with multiplex assays and detection in complex bio-fluids, such as whole blood or a pool of nucleic acids, without purification in advance. With a simplified operation procedure, low instrumentation requirement, high sensitivity and compatibility with complex bio-fluids, this method provides an ideal solution for visual detection of nucleic acids in resource-limited settings.

Introduction

Short, single-stranded nucleic acids often serve as biomarkers of disease and bioterrorism agents. Their detection has broad applications, such as in pathogen identification[1–4] and disease diagnosis.[5,6] Many platforms have been developed for detecting nucleic acid molecules with specific sequences, including polymerase chain reaction (PCR),[7–14] bio-barcode-based detection[15,16] and electrochemistry.[17,18] PCR-based methods, in particular, have been largely used to detect nucleic acids in ultra-low abundance. However, this approach requires labour-intensive procedures and cumbersome instrumentation. These limitations have created significant challenges in healthcare medication in developing countries and other resource-limited sites. For example, the recent Ebola virus outbreak in Africa was partially due to the lack of diagnostic facilities in many local hospitals and clinics.[19] Thus, effective detection and diagnosis, suitable for low-resource settings, is of particular importance.

It is clear that there is a high demand for a simple and efficient approach. In recent years, the development of visual detection methods based on gold nanoparticles (AuNPs),[20–26] silver nanoparticles[27] and graphene oxide[28] has increased rapidly because of their simplicity and the visual readouts produced.[29–35] Mirkin and coworkers pioneered a AuNP-based colorimetric assay.[29] Typically, AuNPs have been surface-functionalised with detection probes designed to bind with target molecules.[20,26,29,36,37] Thus, the presence of target molecules induces the aggregation of AuNPs by forming a sandwich-type structure, *i.e.* AuNPs–targets–AuNPs, resulting in a change of the bulk solution colour from red to purple readable by visual inspection or spectrometry.[20,26,29] Numerous methods based on AuNP aggregation have been developed to detect DNAs/RNAs, proteins and metal ions.[26,29,37] Moreover, to improve its sensitivity, enzymatic[38] or non-enzymatic DNA circuits[39,40] were recently employed.[41–44] In addition, a lateral flow strip based on AuNPs was also developed that can provide a fast and visual readout for detection of nucleic acids.[45,46] In particular, by using magnetic microparticles (MMPs) the AuNP-based assay was developed into a magnetophoretic assay with a significantly reduced detection time and

[a]*Department of Mechanical and Biomedical Engineering, City University of Hong Kong, Hong Kong Special Administrative Region, China.*
E-mail: thchen@cityu.edu.hk; Fax: (+852) 34420172; Tel: (+852) 34424114
[b]*School of Creative Media, City University of Hong Kong, Hong Kong Special Administrative Region, China*
[c]*Centre for Robotics and Automation, City University of Hong Kong, Hong Kong Special Administrative Region, China*

†Electronic supplementary information (ESI) available. See DOI: 10.1039/c5an01123j

a simplified equipment requirement.[47–49] However, although AuNPs are widely used, their modification is time-consuming and requires delicate protocols to stabilise their mono-dispersion. For example, the mono-dispersed AuNPs are sensitive to the ionic strength of the solution.[49,50] Alteration of the ionic strength may result in undesirable aggregation, creating additional uncertainty in optimising the assay sensitivity and repeatability[47,51] and making it incompatible with complex environments such as bio-fluids. On the other hand, the intrinsic colour of a biological sample can create significant interference for colorimetric assays. Consequently, delicate preparation or biomarker purification may be required, which restricts the practicality of the assay.

Here we report on a new visual detection method for nucleic acids, based on Mie scattering and the magnetophoretic effect (Fig. 1). Instead of AuNPs, we used polystyrene microparticles (PMPs) with 1.04 μm diameter as the suspended particles. Two probes, P1 and P2, were designed to hybridise in juxtaposition with a target oligonucleotide. As such, using MMPs modified with P1 and PMPs modified with P2, the present target oligonucleotides led to the formation of an MMPs–targets–PMPs sandwich structure, which was attracted to the sidewall when an external magnet was attached, thus changing the solution turbidity from opaque to transparent. Importantly, the change in turbidity was caused by the Mie scattering due to the size of the PMPs, which could effectively attenuate the light transmission[52,53] with a significantly enhanced extinction coefficient compared to AuNPs (~3 orders of magnitude, Fig. S1†). In addition, PMPs showed improved stability in their dispersion, rapid modification through a streptavidin–biotin link and enhanced compatibility with complex bio-fluids. Based on the enhanced light scattering effect and stability, this method achieved a limit of detection at 16 pM by the naked eye and at 4 pM by spectrometry. In addition, it is compatible with multiplex assays and detection in complex bio-fluids, such as whole blood or a pool of nucleic acids, without purification in advance. With its simple procedure, low instrumentation requirement and sufficient sensitivity, this method provides an ideal solution for applications in resource-limited settings.

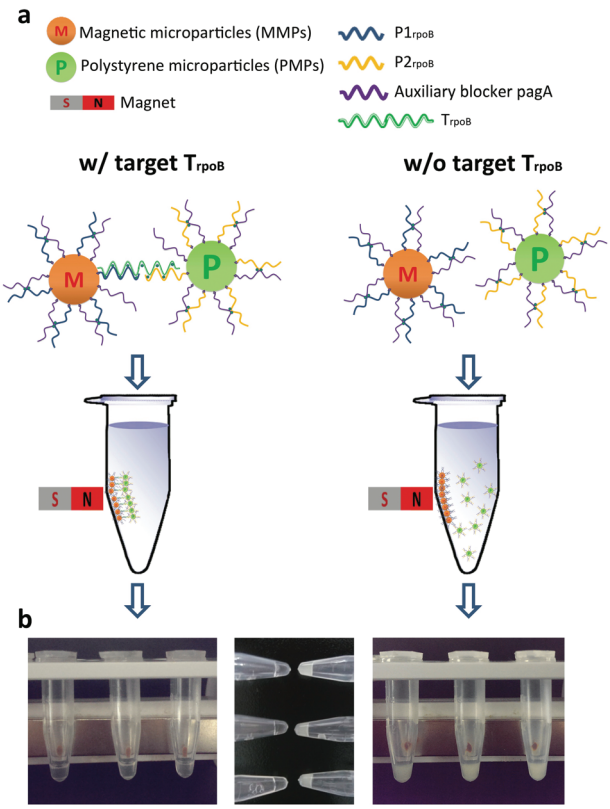

Fig. 1 Operating principle for the visual detection of nucleic acids. (a) Two types of microparticles were used: magnetic microparticles (MMPs) modified with both $P1_{rpoB}$ + pagA and polystyrene microparticles (PMPs) modified with $P2_{rpoB}$ + pagA. When the target oligonucleotides, T_{rpoB}, hybridise with the $P1_{rpoB}$ and $P2_{rpoB}$ in juxtaposition, MMPs and PMPs link together, such that an externally applied magnetic field can attract MMPs and the linked PMPs, yielding a change in light transmission and solution turbidity *via* Mie scattering. (b) Optical images showing the changes in light transmission in response to the presence of the target, T_{rpoB}. When T_{rpoB} was present, the solution became transparent (left). In contrast, when target T_{rpoB} was absent, the solution remained opaque (right).

Materials and methods

Oligonucleotide sequences

Single-stranded oligonucleotides were purchased from Sangon Biotech Ltd (Shanghai, China) and dissolved in Tris-ethylenediaminetetraacetic acid (Tris-EDTA) buffer. The sequences are listed in Tables 1 and S1.† Oligonucleotide probes, $P1_{rpoB}$ pairing with $P2_{rpoB}$ and $P1_{capC}$ pairing with $P2_{capC}$, were designed with a sequence complementary to the target oligonucleotides T_{rpoB} and T_{capC}, respectively, in juxtaposition. T_{rpoB} + 30A and T_{rpoB} + 60A are targets of which 30 bases and 60 bases of adenine (A) were inserted in the middle of the sequence of T_{rpoB}, respectively (Table S1†). The SNP A, SNP G and SNP C oligonucleotides were designed with single-base mismatches (shown in bold italics in Table 1) compared to T_{rpoB}. The probes and the auxiliary blocker oligonucleotide, pagA, were biotinylated, such that they can spontaneously

Table 1 The sequences of the single-strand oligonucleotides

Strand name	Sequence
T_{rpoB}	5′-ACTTGTGTCTCGTTTCTTCGATCCAAAGCG-3′
$P1_{rpoB}$	5′-AAACGAGACACAAGT-/biotin/-3′
$P2_{rpoB}$	5′-/biotin/CGCTTTGGATCGAAG-3′
pagA	5′-CTCGAACTGGAGTGA-/biotin/-3′
T_{capC}	5′-ATGCCATTTGAGATTTTTGAATTCCGTGGT-3′
$P1_{capC}$	5′-AATCTCAAATGGCAT-/biotin/-3′
$P2_{capC}$	5′-/biotin/-ACCACGGAATTCAAA-3′
SNP A	5′-ACTTGTG***A***CTCGTTTCTTCGATCCAAAGCG-3′
SNP G	5′-ACTTGTG***G***CTCGTTTCTTCGATCCAAAGCG-3′
SNP C	5′-ACTTGTG***C***CTCGTTTCTTCGATCCAAAGCG-3′

attach to streptavidin-coated MMPs of 0.90 μm (CM01N, Bangslab, USA) and streptavidin-coated PMPs of 1.04 μm (CP01F, Bangslab, USA) and 0.97 μm.

Modification of microparticles

Based on the streptavidin–biotin bonds, the MMPs were modified with $P1_{rpoB}$ and pagA, while the PMPs were modified with $P2_{rpoB}$ and pagA. Briefly, a 3.5 μl suspension of MMPs (10 mg ml^{-1}) was mixed with 2.5 μg $P1_{rpoB}$ and 2.5 μg pagA. A 3.5 μl suspension of PMPs (10 mg ml^{-1}) was mixed with 2.5 μg $P2_{rpoB}$ and 2.5 μg pagA. The mixtures were incubated for 30 min at room temperature with gentle shaking, allowing immobilisation of biotinylated oligonucleotides on streptavidin-coated microparticles. Next, the MMPs and PMPs were rinsed with 200 μl of wash buffer (20 mM Tris-HCl, pH 7.5, 1 M NaCl, 1 mM EDTA, 0.0005% Trition X-100) three times to remove the residual oligonucleotides. For each washing step, the MMPs were collected using a magnetic separation rack, while the PMPs were collected using a centrifuge (13.8*g* for 5 min).

PMP-based magnetophoretic assay

Two protocols were used. The modified MMPs and PMPs (35 μg each) were first mixed in 20 μl of hybridisation buffer (10 mM Tris-HCl, 1 mM EDTA, 1 M NaCl, 0.2% Tween 20, pH 8.2) and the supernatant was removed after centrifugation (13.8*g* for 5 min). In the first protocol, 20 μl of hybridisation buffer with varying concentrations of the target T_{rpoB}, T_{rpoB} + 30A, T_{rpoB} + 60A, SNP A, SNP G or SNP C was mixed with MMPs and PMPs for 30 min at room temperature with gentle shaking. In the second protocol, 1500 μl of hybridisation buffer with varying concentrations of target T_{rpoB} was first mixed with 35 μg of MMPs for 30 min at room temperature with gentle shaking. The MMPs were then washed and separated from the suspension using a magnetic separation rack and the MMPs with T_{rpoB} were mixed with the modified PMPs (35 μg) in 20 μl of hybridisation buffer for 30 min with gentle shaking. Finally, a magnetic separation rack or a magnet was used to provide magnetic attraction that pulls the MMPs and MMPs–targets–PMPs towards the sidewall, allowing the solution turbidity observed by the naked eye or quantitatively analysed using a UV-Vis spectrometer (BioDrop μLITE, UK).

Multiplex assay

The MMPs were simultaneously modified with $P1_{rpoB}$ and $P1_{capC}$, to capture targets T_{rpoB} and T_{capC}, respectively. The PMPs of 1.04 μm diameter were modified with $P2_{rpoB}$ and pagA, while the PMPs of 0.97 μm diameter were modified with $P2_{capC}$ and pagA. Briefly, a 3.5 μl suspension of MMPs (10 mg ml^{-1}) was mixed with 2.5 μg $P1_{rpoB}$ and 2.5 μg $P1_{capC}$. A 3.5 μl suspension of 1.04 μm diameter PMPs (10 mg ml^{-1}) was mixed with 2.5 μg $P2_{rpoB}$ and 2.5 μg pagA. Similarly, a 3.5 μl suspension of 0.97 μm diameter PMPs (10 mg ml^{-1}) was mixed with 2.5 μg $P2_{capC}$ and 2.5 μg pagA. These mixtures were incubated for 30 min at room temperature with gentle shaking and the MMPs and two types of modified PMPs were then rinsed with 200 μl of wash buffer, three times, to remove the residual oligonucleotides. For each washing step, the MMPs were collected using a magnetic separation rack, while the PMPs were collected by centrifugation (13.8*g* for 5 min). Next, 1500 μl of hybridisation buffer with different types of target oligonucleotides (a blank sample containing only a buffer solution, T_{rpoB}, T_{capC} or T_{rpoB} + T_{capC}) at 50 pM was first mixed with the MMPs and incubated for 30 min at room temperature with gentle shaking. The MMPs were then separated from the suspension using a magnetic separation rack. Subsequently, the suspension of two types of modified PMPs was mixed with the MMPs in 20 μl of hybridisation buffer and the mixture was incubated for 30 min at room temperature with gentle shaking. Finally, a magnetic separation rack or a magnet was used to provide magnetic attraction removing the MMPs and MMPs–targets–PMPs from the suspension, and the solution turbidity was quantitatively analysed using a UV-Vis spectrometer.

Detection in a complex bio-fluid environment

MMPs and PMPs modified with probes recognising T_{rpoB} were prepared as described. Next, 1500 μl of rabbit whole blood (Qiyi Biological Technology Co., Ltd) or a solution of nucleic acid pool isolated from human mammary gland metastatic epithelial cells (MDA-MB-231, see the ESI†), with varying concentrations of the target T_{rpoB}, was mixed with 35 μg of MMPs and incubated for 30 min at room temperature with gentle shaking. The MMPs were then collected from the bio-fluid using a magnetic separation rack and rinsed in 1500 μl of wash buffer, three times, to remove the residual rabbit blood. This step removed the target T_{rpoB} from the interference of the bio-fluid environment. Afterwards, the MMPs were mixed with 35 μg of modified PMPs in 20 μl of hybridisation buffer and incubated for 30 min at room temperature with gentle shaking. A magnetic separation rack or a magnet was used for magnetic attraction, and the solution turbidity was observed directly by the naked eye or quantified using a UV-Vis spectrometer.

Results

Operating principle

The schematic is shown in Fig. 1a. To detect the target T_{rpoB}, the biotinylated oligonucleotides, $P1_{rpoB}$ and $P2_{rpoB}$, were designed with sequences complementary to T_{rpoB}, in juxtaposition. $P1_{rpoB}$ and $P2_{rpoB}$ were immobilised onto streptavidin-coated MMPs and PMPs, respectively, *via* biotin–streptavidin interactions. As such, when T_{rpoB} was present, $P1_{rpoB}$ and $P2_{rpoB}$ hybridised with T_{rpoB} simultaneously, forming a sandwich-like structure, MMPs–T_{rpoB}–PMPs. Thus, using a magnetic field, the PMPs were carried by the MMPs towards the sidewall, making the suspension transparent (Fig. 1b). In contrast, when T_{rpoB} was absent, the PMPs were freely suspended in the solution, which made the suspension opaque due to the Mie scattering.

We first investigated whether there was any non-specific binding if only $P1_{rpoB}$ and $P2_{rpoB}$ were used. The MMPs modi-

fied with $P1_{rpoB}$ and the PMPs modified with $P2_{rpoB}$ were mixed in 20 μl of hybridisation buffer and the suspension was placed onto a magnetic separation rack. The results showed that the suspension rapidly became transparent (Fig. 2). Using a UV-Vis spectrometer, the measurement yielded a low absorbance at 400 nm, indicating strong non-specific binding between MMPs and PMPs, even though the target T_{rpoB} was absent (Fig. 2). We hypothesised that the partial complementary sequence between $P1_{rpoB}$ and $P2_{rpoB}$, "5′-AAA-3′" on $P1_{rpoB}$ pairing with "3′-TTT-5′" on $P2_{rpoB}$ or "5′-CGA-3′" on $P1_{rpoB}$ pairing with "3′-TCG-5′" on $P2_{rpoB}$, could be the reason for such spontaneous binding between MMPs and PMPs. To verify this, the modification of PMPs was changed to $P2_{capC}$, which has no sequence complementary with $P1_{rpoB}$. After magnetic attraction, the suspension remained opaque, validating that the strong non-specific binding between $P1_{rpoB}$- and $P2_{rpoB}$-modified microparticles was due to the hybridisation of partial complementary sequences.

To avoid this non-specific binding, a biotinylated auxiliary oligonucleotide (pagA) was introduced. The sequence of pagA was partially complementary to $P1_{rpoB}$ at "5′-CTCG-3′" and $P2_{rpoB}$ at "5′-TCGA-3′". Therefore, pagA could partially hybridise with $P1_{rpoB}$ and $P2_{rpoB}$. As such, when T_{rpoB} was present, the partial hybridisation denatured and $P1_{rpoB}$ and $P2_{rpoB}$ can then hybridise with T_{rpoB} in juxtaposition, forming sandwich structures that make the suspension transparent through the magnetophoretic effect. To demonstrate the feasibility of this mechanism, we used MMPs modified with $P1_{rpoB}$ and pagA, and PMPs modified with $P2_{rpoB}$ and pagA. The result showed that the non-specific binding was eliminated (Fig. 2).

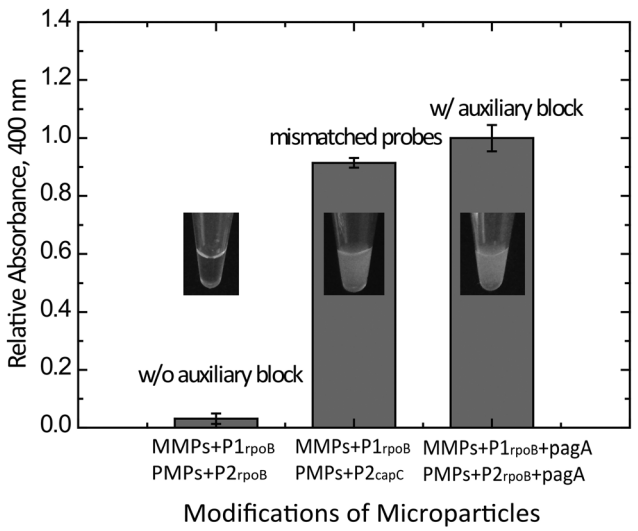

Fig. 2 Elimination of non-specific binding between MMPs and PMPs. Optical images and relative UV-Vis spectral absorbance at 400 nm showing that, for MMPs modified with $P1_{rpoB}$ and PMPs modified with $P2_{rpoB}$, the partial hybridisation between $P1_{rpoB}$ and $P2_{rpoB}$ led to non-specific binding and made the suspension transparent, even when the target oligonucleotides were absent. This non-specific binding can be eliminated using MMPs modified with $P1_{rpoB}$ + pagA and PMPs modified with $P2_{rpoB}$ + pagA, where auxiliary oligonucleotide pagA was able to block the partial hybridisation, or using a pair of oligonucleotide probes that have no partial hybridisation, such as $P1_{rpoB}$ and $P2_{capC}$. The absorbance of the suspension resulting from the modification with the auxiliary block was used as the reference. The relative absorbance is from repeated experiments (mean ± SEM, n = 3).

We next tested the limit of detection using 20 μl of T_{rpoB} solution at various concentrations (0 M, 0.05 nM, 0.5 nM, 1 nM, 2 nM, 3 nM, 4 nM, 5 nM, 10 nM, 20 nM and 50 nM). The suspension from 0 M was completely opaque. In contrast, as the concentration of T_{rpoB} increased, the suspension gradually became transparent. The difference can be discriminated by the naked eye when concentrations of T_{rpoB} were greater than 2 nM (Fig. 3a). Using a UV-Vis spectrometer, the spectral absorbance of the suspension was analysed (Fig. 3b and c). According to the absorbance at 400 nm, the limit of detection was 50 pM. Note that the absorbance was inversely proportional to the concentration of T_{rpoB} and had a linear range of 50 pM–2 nM (R^2 = 0.997, Fig. 3d). Moreover, in this detection strategy, the MMPs and PMPs were used as the final detecting agents to directly react with the target solution in 20 μl. Thus, the duration was only 10–30 min. When the concentration of the target oligonucleotide was high, detection was almost in real-time and was visible to the naked eye.

Moreover, to test whether the detection is applicable to longer target oligonucleotides, we designed the sequences of T_{rpoB} + 30A and T_{rpoB} + 60A, of which 30 bases and 60 bases of adenine (A) were inserted in the middle of the sequence of T_{rpoB}, respectively (Table S1†). The results showed that the suspensions resulting from 10 nM of T_{rpoB}, T_{rpoB} + 30A and T_{rpoB} + 60A became all transparent and had a similar level of absorbance (Fig. S3†), indicating the compatibility with the detection of targets with a longer length.

Optimisation of experimental conditions

Considering that target molecules are mostly present in more dilute and complex environments, we next optimised the experimental protocol to adapt to these. Magnetic particles have been frequently used for extraction and purification of target molecules.[54,55] Thus, the magnetophoretic assay was performed into two steps: (1) target oligonucleotide extraction and (2) visual detection. After preparation of MMPs and PMPs, the MMPs were first used to extract the T_{rpoB} from a diluted sample solution of a larger volume, *e.g.* 1500 μl. After incubation and washing, the PMPs were then introduced into the MMPs carrying the target T_{rpoB}, followed by visual detection of the suspension using magnetic attraction. Lower concentrations of the T_{rpoB} solution were used, including 0 M, 4 pM, 10 pM, 16 pM, 32 pM, 64 pM and 128 pM. The results showed that when using MMPs for target extraction, the limit of detection was reduced to 4 pM by the spectrum analysis (Fig. 4a and b) and 10 pM by visual inspection. Meanwhile, the spectral absorbance decreased as the concentration of T_{rpoB} increased (Fig. 4c), with a linear range of 4 pM–128 pM detected using a UV-Vis spectrometer (Fig. 4d).

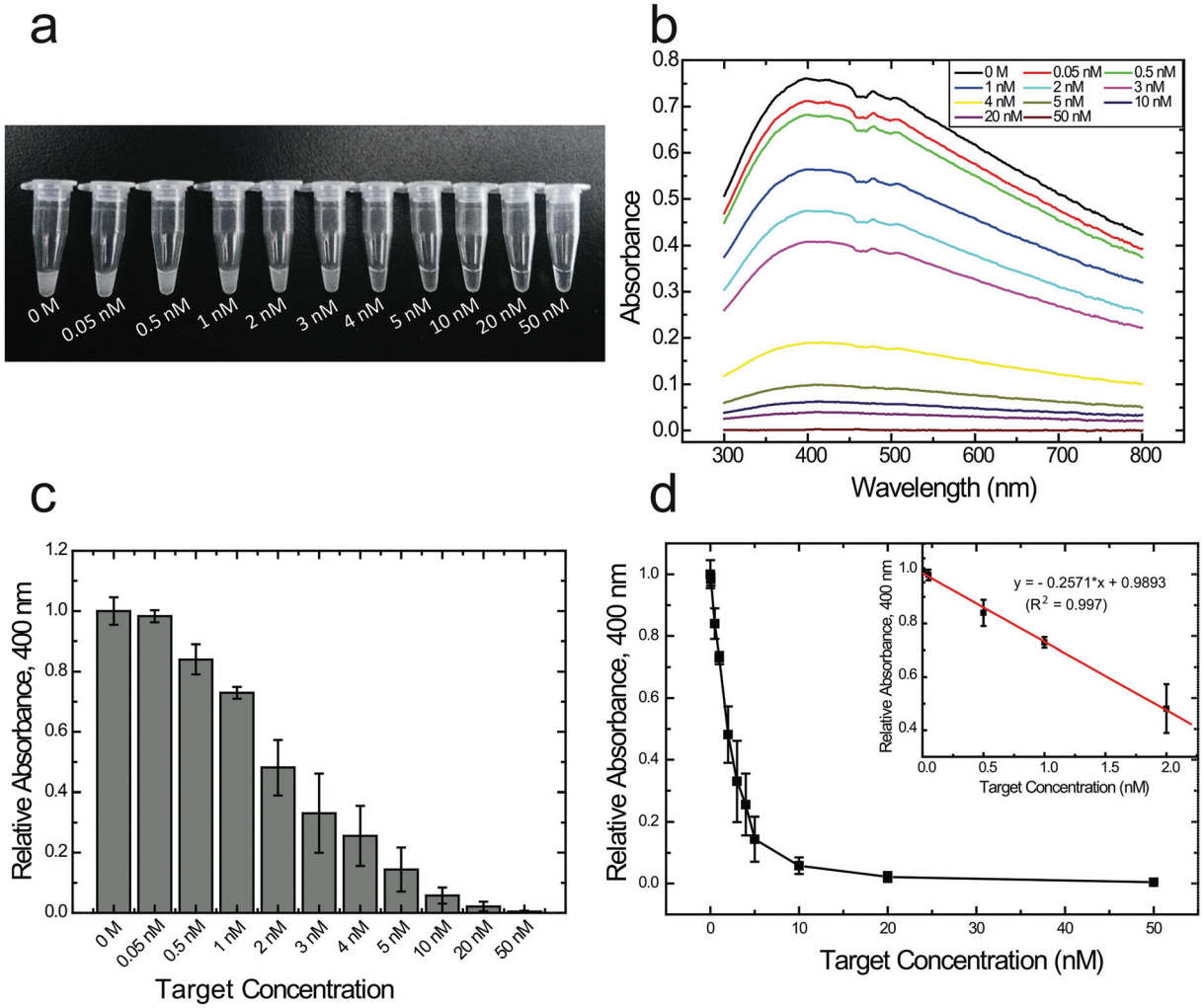

Fig. 3 Detection of T_{rpoB} solution of varying concentrations. (a) Optical images showing the changes in solution turbidity in response to different concentrations of T_{rpoB}. (b) UV-Vis spectral absorbance of the suspension of (a). (c) Relative UV-Vis spectral absorbance at 400 nm of the suspension from repeated experiments (mean ± SEM, n = 3). (d) Analysis of the relative UV-Vis spectral absorbance at 400 nm of the suspension resulting from varying concentrations of T_{rpoB}. Inset: the linear range between the concentration of T_{rpoB} and the relative UV-Vis spectral absorbance at 400 nm. The absorbance of the suspension resulting from the blank sample (hybridisation buffer with 0 M target oligonucleotides) was used as the reference.

Multiplex assay

On the basis of the optimised experimental conditions, we next explored the possibility of multiplex detection for two types of target molecules, T_{rpoB} and T_{capC}. We first tested the specificity of this assay by analysing single nucleotide polymorphisms (SNPs). SNP A, SNP G and SNP C were designed based on the target oligonucleotides T_{rpoB} but with the eighth nucleotide, T, replaced by A, G or C (Table 1). The results showed that although the relative absorbance for the solutions of SNP A, SNP G and SNP C was slightly lower compared to the blank sample (hybridisation buffer with 0 M of the target), they were significantly different from that of T_{rpoB} (Fig. 5), indicating their ability to differentiate target oligonucleotides with single nucleotide mismatched sequences.

For the multiplex assay, a second type of PMP with 0.97 μm diameter was introduced to detect T_{capC}. As PMPs differ in size, the spectrum of absorbance in the suspension of PMPs showed a red shift (Fig. S2†), providing signal characters for multiplex assays. We used the 0.97 μm diameter PMPs modified with $P2_{capC}$ and pagA to detect T_{capC} and the 1.04 μm diameter PMPs modified with $P2_{rpoB}$ and pagA to detect T_{rpoB}. The MMPs were simultaneously modified with $P1_{capC}$ and $P1_{rpoB}$. Before exposure to T_{rpoB} or T_{capC}, the mixed particle suspension showed an absorbance peak near 379 nm (Fig. 6). However, when the solution of T_{rpoB} at 50 pM was mixed with the particles, after incubation, magnetic attraction only pulled the 1.04 μm diameter PMPs to the sidewall, leaving the 0.97 μm diameter PMPs suspended and the absorbance peak shifted from 379 nm to 364 nm. In contrast, for the solution containing only T_{capC}, only the 0.97 μm diameter PMPs were magnetically attracted, shifting the absorbance peak to 396 nm. In addition, when both T_{rpoB} and T_{capC} were present, both kinds of PMPs were attracted to the sidewall, resulting in

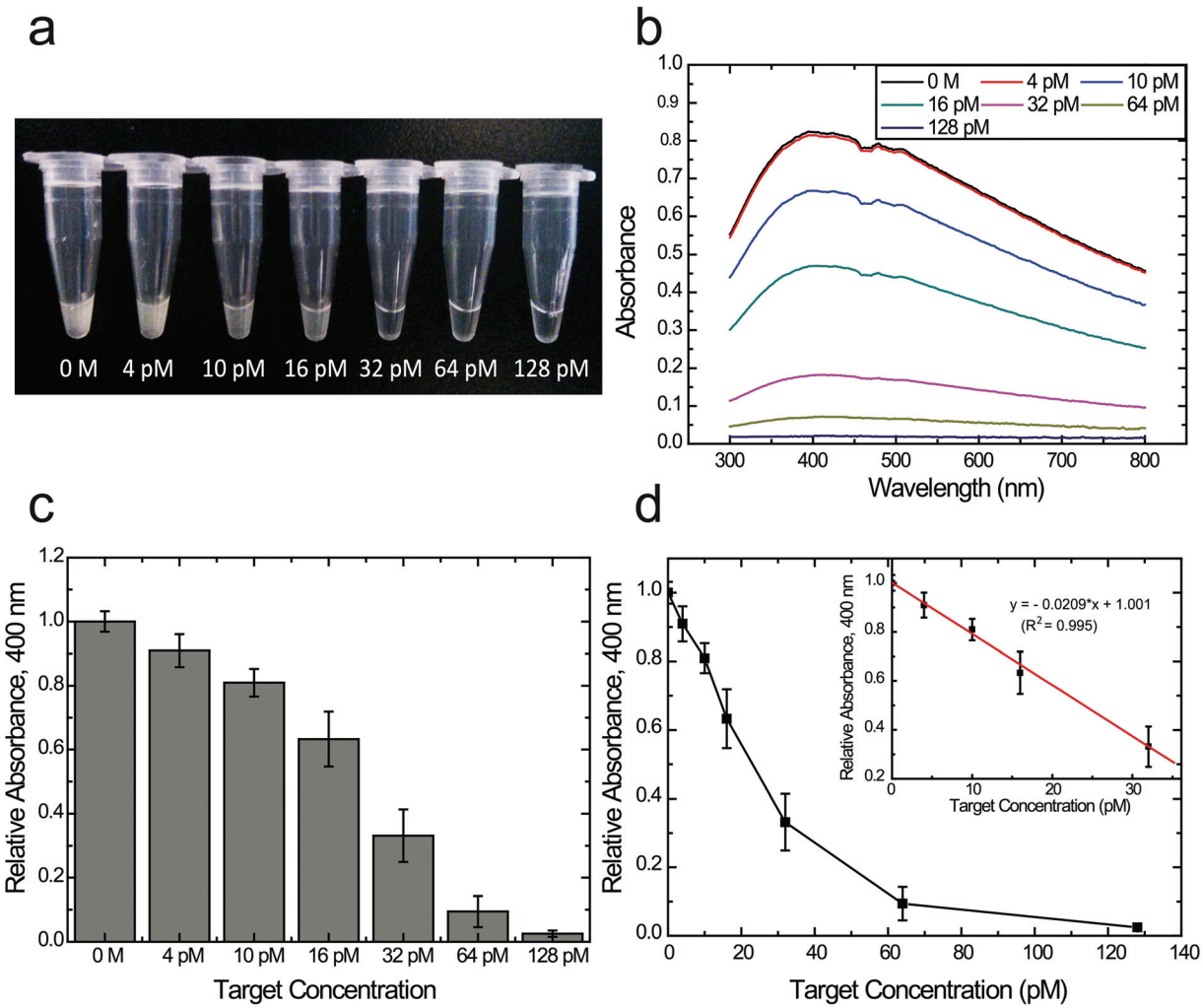

Fig. 4 Detection of diluted T_{rpoB} solution using optimised experimental conditions. (a) Optical images showing the changes in solution turbidity in response to the concentrations of T_{rpoB}. (b) UV-Vis spectral absorbance of the suspension of (a). (c) Relative UV-Vis spectral absorbance at 400 nm of the suspensions from repeated experiments (mean ± SEM, n = 3). (d) Analysis of the relative UV-Vis spectral absorbance at 400 nm of the suspension resulting from varying concentrations of T_{rpoB}. Inset: the linear range between the concentration of T_{rpoB} and the relative UV-Vis spectral absorbance at 400 nm. The absorbance of the suspension resulting from the blank sample (hybridisation buffer with 0 M target oligonucleotides) was used as the reference.

a transparent suspension with nearly zero absorbance. Thus, these combinatory experiments demonstrate that this PMP-based magnetophoretic assay is capable of multiplex detection of target oligonucleotides at concentrations as low as 50 pM.

Detection in a complex bio-fluid environment

Nucleic acid biomarkers such as microRNAs, short oligonucleotides present in the blood stream, were recently found to show promise for cancer classification and prognostication.[56] However, for other visual detection methods based on AuNPs, the dispersion of AuNPs may be unstable due to interfering materials in whole blood, such as cells, DNAs/RNAs and proteins. Moreover, the intrinsic colour of whole blood causes significant interference for the colorimetric readout, creating considerable challenges for detection sensitivity and stability. Therefore, before the assay, extraction and purification of biomarkers is usually required, which is difficult for point-of-care applications.

To demonstrate the stability of our assay in complex environments, we next investigated whether the optimised visual assay was compatible with complex bio-fluids. Compared to AuNPs, one of the advantages of using PMPs is the stability of the particle suspension and the tolerance to interfering biomolecules. We first conducted detection under the interference from a pool of nucleic acids isolated from human mammary gland metastatic epithelial cells (MDA-MB-231, see the ESI†). Using the optimised protocol, T_{rpoB} was extracted with MMPs, followed by washing steps to remove the residual bio-fluid *via* magnetic separation. The MMPs with extracted T_{rpoB} were then mixed with the PMPs for the magnetophoretic assay. One hundred pM of T_{rpoB} was mixed with 641 ng ml^{-1}

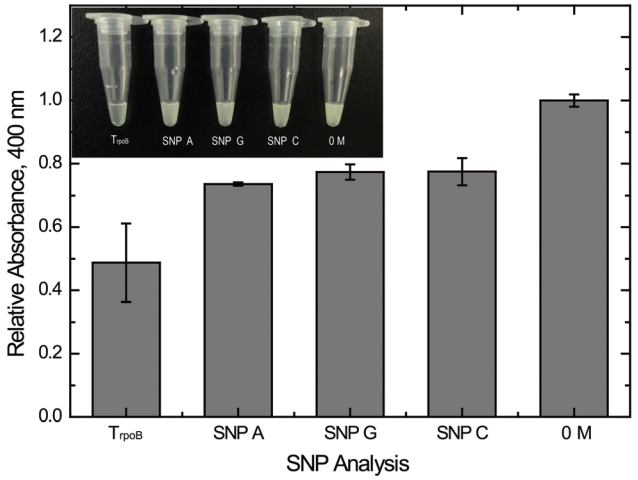

Fig. 5 Single nucleotide polymorphism (SNP) analysis. Optical images and relative UV-Vis spectral absorbance of the suspensions resulting from 5 nM of T_{rpoB} or SNP A, SNP G or SNP C, at 400 nm. For SNP A, SNP G and SNP C the eighth nucleotide, T, of T_{rpoB} was replaced by A, G or C, respectively. The absorbance of the suspension resulting from the blank sample (hybridisation buffer with 0 M target oligonucleotides) was used as the reference. The relative absorbance is from repeated experiments (mean ± SEM, n = 3).

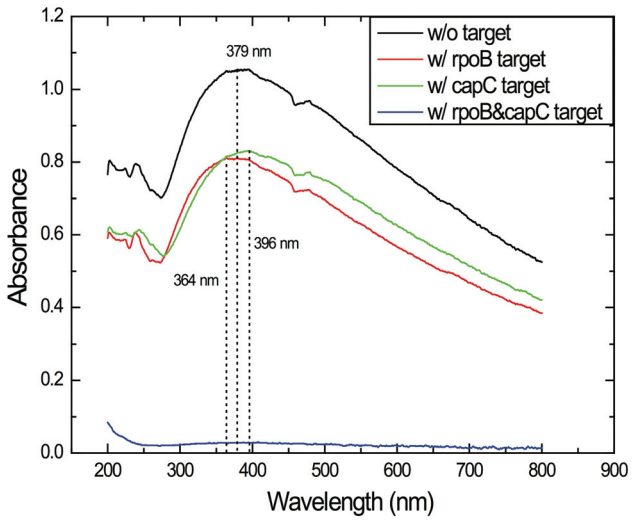

Fig. 6 Multiplex detection of T_{rpoB} and T_{capC}. Conducted with MMPs modified with $P1_{rpoB}$ + $P1_{capC}$, 0.97 μm-diameter PMPs modified with $P2_{capC}$ + pagA for detecting T_{capC}, and 1.04 μm-diameter PMPs modified with $P2_{rpob}$ + pagA for detecting T_{rpoB}, the spectral absorbance showed a peak at 379 nm when the target oligonucleotide was absent; it shifted to 364 nm when exposed to T_{rpoB} solution at 50 pM, and to 396 nm when exposed to T_{capC} solution at 50 pM. When exposed to both T_{rpoB} and T_{capC}, the solution became transparent.

RNAs extracted from the cell lysate. The result showed that the presence of interfering molecules does not hinder the detection (Fig. 7a).

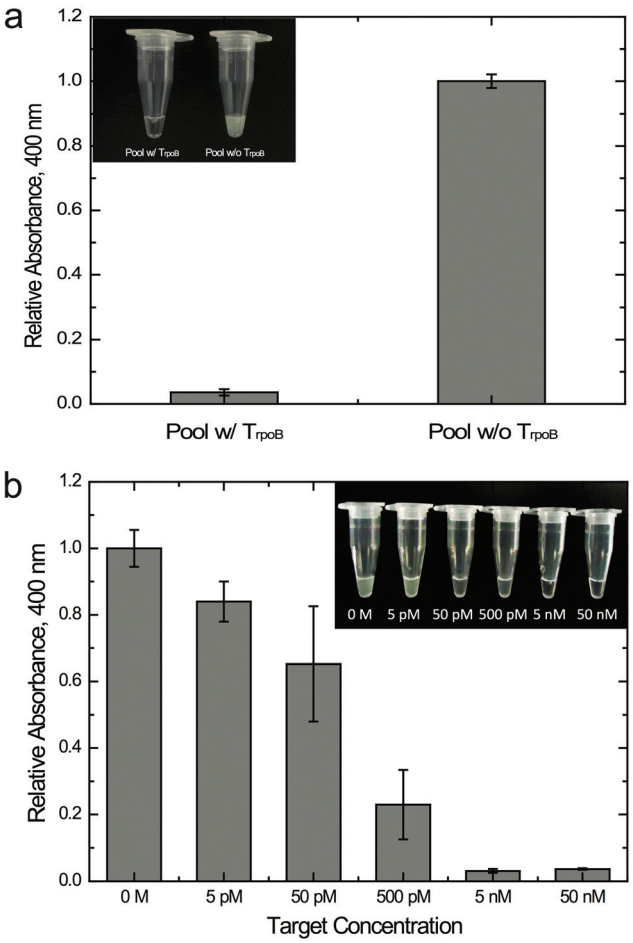

Fig. 7 Detection in a complex bio-fluid environment. (a) Optical images and relative UV-Vis spectral absorbance at 400 nm showing the changes of solution turbidity when T_{rpoB} was present at 100 pM or absent in the nucleic acid pool. The absorbance resulting from the blank sample (solution of nucleic acid pool without target oligonucleotides) was used as the reference. The relative absorbance is from repeated experiments (mean ± SEM, n = 3). (b) Optical images and relative UV-Vis spectral absorbance at 400 nm showing the changes in solution turbidity with varying concentrations of T_{rpoB}. The absorbance of the suspension resulting from the blank sample (hybridisation buffer with 0 M target oligonucleotides) was used as the reference. The relative absorbance is from repeated experiments (mean ± SEM, n = 3).

Furthermore, to demonstrate the compatibility with the whole blood environment, we used the target molecule T_{rpoB} mixed in undiluted rabbit blood at concentrations of 0 M, 5 pM, 50 pM, 500 pM, 5 nM and 50 nM. The results showed that, although the total absorbance was reduced, possibly caused by non-specific binding of the complex components of blood, we still achieved a limit of detection as low as 50 pM by visual inspection and 5 pM by UV-Vis spectral analysis (Fig. 7b). Altogether, these results demonstrated that our PMP-based magnetophoretic assay is compatible with complex bio-fluids, and retains its high sensitivity without the need for additional purification processes, indicating its potential for future practical applications such as on-site examination.

Discussion

This approach has many advantages over the most recent visual detection methods for nucleic acids, as compared in Table 2. The use of magnetic microparticles offers an extremely convenient and economical method for processing complex sample solutions by extracting and purifying the diluted nucleic acid targets from complex fluids. PMPs also have the advantage of greatly enhanced suspension stability, which is important for the visual detection of biomarkers in complex bio-fluids. In addition, compared to methods using AuNPs, which require time-consuming modification (~16 hours) and delicate protocols to stabilise their mono-dispersion, the effective streptavidin–biotin links for the modification of PMPs offer a much more efficient and stable approach.

In addition to the stability and convenience of our method, the enhanced extinction coefficient due to the Mie scattering by PMPs provides a limit of detection lower than, or comparable to, the AuNP-based method (50 pM).[47] The Mie scattering describes a phenomenon where an electromagnetic plane wave passes by homogeneous spheres, the size of which is comparable to the wavelength of light.[57–61] When a light beam passes a solution, the intensities of the incident and scattered light together with the absorbed beam follow Lambert–Beer's law:

$$A_\lambda = \varepsilon c L$$

where $A_\lambda = \mathrm{In}(I_i/I_o)$ is the spectral absorbance at the wavelength λ, I_i is the intensity of the incident beam, I_o is the intensity of the beam passing through the solution, ε is the extinction coefficient, c is the concentration of PMPs in the suspension and L is the pathlength of light. The extinction coefficient ε for spheres is a function of size parameter $\pi d/\lambda$. When the diameter d is 600–1200 nm, λ = 546.1 nm and the refractive index n = 1.333, ε reaches a high value range of specific turbidity.[59] Measured using a UV-Vis spectrometer at 400 nm for a series dilution of PMP suspension, we calculated the extinction coefficient ε as 4.457×10^{12} M^{-1} cm^{-1} (Fig. S1†), which is 3 orders of magnitude greater than that of AuNPs (typically at the scale of 10^9 M^{-1} cm^{-1} for a diameter of 20–40 nm[62]). Thus, although larger PMPs may need more targets to form the particle–particle connection, the significantly enhanced extinction coefficient compensates this shortcoming, making the assay as sensitive as that of AuNP-based assays.

In this magnetophoretic assay, we found that the partial complementary sequence between the oligonucleotide probes resulted in non-specific binding. As the sequence of probes $P1_{rpoB}$ and $P2_{rpoB}$ was based on the sequence of T_{rpoB}, it is difficult to adjust the sequence without changing the hybridisation efficiency. Here we demonstrate that such a partially complementary sequence can be blocked using the auxiliary oligonucleotide, pagA. By calculating the binding energy, we determined the binding energy for $P1_{rpoB}$ + pagA and $P2_{rpoB}$ + pagA as −6.78 kal mol^{-1} and −6.76 kal mol^{-1}, respectively. Note that these were lower than the binding energy between $P1_{rpoB}$ and $P2_{rpoB}$ (−5.19 kal mol^{-1}), indicating that the non-specific binding due to $P1_{rpoB}$ and $P2_{rpoB}$ could be minimised when the auxiliary oligonucleotide pagA was used. As such, this strategy may be further applied to the design of oligonucleotide-based probes for other applications.

For the SNP analysis, the hybridization energy between SNP A, G, or C and $P1_{rpoB}$ is −12.02 kcal mol^{-1}, which is much greater than the hybridization energy, −25.07 kcal mol^{-1}, between T_{rpoB} and $P1_{rpoB}$. Accordingly, the single base mismatch leads to a significant decrease of the binding strength between MMPs and PMPs. For the PMP-based magnetophoretic assay, the flow of PMPs was driven by the movement of MMPs but also resisted by the friction following Stokes' law, $F = 6\pi\mu rV$, where μ is the dynamic viscosity, r is the radius of microparticles, and V is the particle velocity. For PMPs with a diameter of 1.04 μm, this friction is significantly larger than that of the commonly used nanoparticles (~2 orders of magnitude greater). Thus, the weaker connections due to SNP A, G or C were more vulnerable during magnetophoretic flow, which

Table 2 Comparison of visual detection of nucleic acids

Readout	Strategy	Limit of detection	Advantages/drawbacks
Visual (this work)	Mie scattering & the magnetophoretic effect	10 pM (naked eye)	Simple operation; rapid modification by streptavidin–biotin binding; compatibility with complex bio-fluids such as whole blood
Visual[46]	Lateral flow	60 pM (naked eye)	Simple and rapid procedure; time-consuming modification of AuNPs; incompatibility with coloured samples;
Colorimetric[49]	AuNPs & the magnetophoretic effect	100 pM (naked eye)	Time-consuming modification of AuNPs; incompatibility with coloured samples; delicate protocols to stabilise AuNPs' mono-dispersion
Colorimetric[26]	AuNPs & conjugated polyelectrolyte	~1 pM (naked eye)	High sensitivity; incompatibility with coloured samples; delicate protocols to stabilise AuNPs' mono-dispersion
Colorimetric[41,43]	AuNPs & DNA circuit	200 pM in the HCR[a] system and 14 pM in the CHA[b] system (calculated);[41] 25 pM (naked eye)[43]	Time-consuming modification of AuNPs; incompatibility with coloured samples; delicate protocols to stabilise AuNPs' mono-dispersion

[a] HCR: hybridization chain reaction. [b] CHA: catalyzed hairpin assembly.

would lead to the differentiation of perfect matched or single-mismatched targets.

Conclusions

In this paper, we demonstrate the visual detection of nucleic acids using the Mie scattering of PMPs and the magnetophoretic effect. Using MMPs and PMPs modified with oligonucleotide probes, the hybridisation between the probes and the target oligonucleotides leads to a sandwich structure that can be attracted by a magnetic field, resulting in a change in solution turbidity. In addition, using magnetic extraction for diluted samples, the optimised protocol achieved a limit of detection of 4 pM by spectrometry and 16 pM by the naked eye, which is much more sensitive than other visual assays, such as lateral flow test strips or AuNP-based assays. More importantly, based on the efficient magnetic extraction and the stability of mono-dispersed PMPs, we demonstrate that this method can be used to perform multiplex assays and for handling complex fluids, such as whole blood, in a single assay. Thus, by satisfying many of the requirements of point-of-care detection, we envision that this method will be applicable to healthcare and environmental monitoring in resource-limited settings in the future.

Acknowledgements

We are pleased to acknowledge support from the National Natural Science Foundation of China (Grant No. 51305375), the Applied Research Grant (Grant No. 9667097) from City University of Hong Kong, and the Early Career Scheme of Hong Kong Research Grant Council (Project No. 21214815).

Notes and references

1 T. Sato, A. Takayanagi, K. Nagao, N. Tomatsu, T. Fukui, M. Kawaguchi, J. Kudoh, M. Amagai, N. Yamamoto and N. Shimizu, *J. Clin. Microbiol.*, 2010, **48**, 2357–2364.
2 K. W. Hsieh, A. S. Patterson, B. S. Ferguson, K. W. Plaxco and H. T. Soh, *Angew. Chem., Int. Ed.*, 2012, **51**, 4896–4900.
3 C. G. Wang, R. Xiao, P. T. Dong, X. Z. Wu, Z. Rong, L. Xin, J. Tang and S. Q. Wang, *Biosens. Bioelectron.*, 2014, **57**, 36–40.
4 H. R. Griffin, A. Pyle, E. L. Blakely, C. L. Alston, J. Duff, G. Hudson, R. Horvath, I. J. Wilson, M. Santibanez-Koref, R. W. Taylor and P. F. Chinnery, *Genet. Med.*, 2014, **16**, 962–971.
5 Y. Li, M. A. R. St John, X. F. Zhou, Y. Kim, U. Sinha, R. C. K. Jordan, D. Eisele, E. Abemayor, D. Elashoff, N. H. Park and D. T. Wong, *Clin. Cancer Res.*, 2004, **10**, 8442–8450.
6 F. Wei, P. B. Lillehoj and C. M. Ho, *Pediatr. Res.*, 2010, **67**, 458–468.
7 L. Miotke, B. T. Lau, R. T. Rumma and H. P. Ji, *Anal. Chem.*, 2014, **86**, 2618–2624.
8 R. K. Saiki, S. Scharf, F. Faloona, K. B. Mullis, G. T. Horn, H. A. Erlich and N. Arnheim, *Science*, 1985, **230**, 1350–1354.
9 C. Atkinson, V. C. Emery and P. D. Griffiths, *J. Virol. Methods*, 2014, **196**, 40–44.
10 G. Piorkowski, C. Baronti, X. de Lamballerie, L. de Fabritus, L. Bichaud, B. A. Pastorino and M. Bessaud, *J. Virol. Methods*, 2014, **202**, 101–105.
11 L. Miotke, B. T. Lau, R. T. Rumma and H. P. Ji, *Anal. Chem.*, 2014, **86**, 4635–4635.
12 R. Martinez, L. Cook, S. Wendt, E. Atienza and K. R. Jerome, *J. Mol. Diagn.*, 2012, **14**, 686–686.
13 J. Zhang, M. Mahalanabis, L. Liu, J. Chang, N. Pollock and C. Klapperich, *Diagnostics*, 2013, **3**, 155–169.
14 M. Luo, N. Li, Y. Liu, C. Chen, X. Xiang, X. Ji and Z. He, *Biosens. Bioelectron.*, 2014, **55**, 318–323.
15 J. M. Nam, S. I. Stoeva and C. A. Mirkin, *J. Am. Chem. Soc.*, 2004, **126**, 5932–5933.
16 J. M. Nam, S. J. Park and C. A. Mirkin, *J. Am. Chem. Soc.*, 2002, **124**, 3820–3821.
17 C. H. Fan, K. W. Plaxco and A. J. Heeger, *Proc. Natl. Acad. Sci. U. S. A.*, 2003, **100**, 9134–9137.
18 W. Cheng, W. Zhang, Y. R. Yan, B. Shen, D. Zhu, P. H. Lei and S. J. Ding, *Biosens. Bioelectron.*, 2014, **62**, 274–279.
19 S. K. Gire, A. Goba, K. G. Andersen, R. S. G. Sealfon, D. J. Park, L. Kanneh, S. Jalloh, M. Momoh, M. Fullah, G. Dudas, S. Wohl, L. M. Moses, N. L. Yozwiak, S. Winnicki, C. B. Matranga, C. M. Malboeuf, J. Qu, A. D. Gladden, S. F. Schaffner, X. Yang, P. P. Jiang, M. Nekoui, A. Colubri, M. R. Coomber, M. Fonnie, A. Moigboi, M. Gbakie, F. K. Kamara, V. Tucker, E. Konuwa, S. Saffa, J. Sellu, A. A. Jalloh, A. Kovoma, J. Koninga, I. Mustapha, K. Kargbo, M. Foday, M. Yillah, F. Kanneh, W. Robert, J. L. B. Massally, S. B. Chapman, J. Bochicchio, C. Murphy, C. Nusbaum, S. Young, B. Birren, D. S. Grant, J. S. Scheiffelin, E. S. Lander, C. Happi, S. M. Gevao, A. Gnirke, A. Rambaut, R. F. Garry, S. H. Khan and P. C. Sabeti, *Science*, 2014, **345**, 1369–1372.
20 R. Kanjanawarut and X. D. Su, *Anal. Chem.*, 2009, **81**, 6122–6129.
21 Y. M. Fang, J. Song, J. S. Chen, S. B. Li, L. Zhang, G. N. Chen and J. J. Sun, *J. Mater. Chem.*, 2011, **21**, 7898–7900.
22 D. Eck, C. A. Helm, N. J. Wagner and K. A. Vaynberg, *Langmuir*, 2001, **17**, 957–960.
23 P. Englebienne, *Analyst*, 1998, **123**, 1599–1603.
24 J. R. Kalluri, T. Arbneshi, S. A. Khan, A. Neely, P. Candice, B. Varisli, M. Washington, S. McAfee, B. Robinson, S. Banerjee, A. K. Singh, D. Senapati and P. C. Ray, *Angew. Chem., Int. Ed.*, 2009, **48**, 9668–9671.
25 M. Zhang, Y. Q. Liu and B. C. Ye, *Chem. Commun.*, 2011, **47**, 11849–11851.
26 F. Xia, X. L. Zuo, R. Q. Yang, Y. Xiao, D. Kang, A. Vallee-Belisle, X. Gong, J. D. Yuen, B. B. Y. Hsu, A. J. Heeger and K. W. Plaxco, *Proc. Natl. Acad. Sci. U. S. A.*, 2010, **107**, 10837–10841.

27 T. Lou, L. Chen, Z. Chen, Y. Wang, L. Chen and J. Li, *ACS Appl. Mater. Interfaces*, 2011, **3**, 4215–4220.
28 Y. Song, K. Qu, C. Zhao, J. Ren and X. Qu, *Adv. Mater.*, 2010, **22**, 2206–2210.
29 R. Elghanian, J. J. Storhoff, R. C. Mucic, R. L. Letsinger and C. A. Mirkin, *Science*, 1997, **277**, 1078–1081.
30 Z. Zhan, C. Cao and S. J. Sim, *Biosens. Bioelectron.*, 2010, **26**, 511–516.
31 C. Cao, X. Li, J. Lee and S. J. Sim, *Biosens. Bioelectron.*, 2009, **24**, 1292–1297.
32 T. A. Taton, C. A. Mirkin and R. L. Letsinger, *Science*, 2000, **289**, 1757–1760.
33 X. Y. Xu, D. G. Georganopoulou, H. D. Hill and C. A. Mirkin, *Anal. Chem.*, 2007, **79**, 6650–6654.
34 Y. Y. Li, H. J. Schluesener and S. Q. Xu, *Gold Bull.*, 2010, **43**, 29–41.
35 N. L. Rosi and C. A. Mirkin, *Chem. Rev.*, 2005, **105**, 1547–1562.
36 Z. Q. Yuan, J. Cheng, X. D. Cheng, Y. He and E. S. Yeung, *Analyst*, 2012, **137**, 2930–2932.
37 F. Wei, R. Lam, S. Cheng, S. Lu, D. A. Ho and N. Li, *Appl. Phys. Lett.*, 2010, 96.
38 J. Li, H. E. Fu, L. J. Wu, A. X. Zheng, G. N. Chen and H. H. Yang, *Anal. Chem.*, 2012, **84**, 5309–5315.
39 R. M. Dirks and N. A. Pierce, *Proc. Natl. Acad. Sci. U. S. A.*, 2004, **101**, 15275–15278.
40 P. Yin, H. M. T. Choi, C. R. Calvert and N. A. Pierce, *Nature*, 2008, **451**, 318–U314.
41 K. Quan, J. Huang, X. H. Yang, Y. J. Yang, L. Ying, H. Wang and K. M. Wang, *Analyst*, 2015, **140**, 1004–1007.
42 K. Quan, J. Huang, X. H. Yang, Y. J. Yang, L. Ying, H. Wang, Y. He and K. M. Wang, *Chem. Commun.*, 2015, **51**, 937–940.
43 C. P. Ma, Z. W. Wu, W. S. Wang, Q. Q. Jiang and C. Shi, *J. Mater. Chem. B*, 2015, **3**, 2853–2857.
44 P. Liu, X. H. Yang, S. Sun, Q. Wang, K. M. Wang, J. Huang, J. B. Liu and L. L. He, *Anal. Chem.*, 2013, **85**, 7689–7695.
45 S. K. Rastogi, C. M. Gibson, J. R. Branen, D. E. Aston, A. L. Branen and P. J. Hrdlicka, *Chem. Commun.*, 2012, **48**, 7714–7716.
46 X. F. Gao, H. Xu, M. Baloda, A. S. Gurung, L. P. Xu, T. Wang, X. J. Zhang and G. D. Liu, *Biosens. Bioelectron.*, 2014, **54**, 578–584.
47 Y. Z. Liu, Z. T. Wu, G. H. Zhou, Z. K. He, X. D. Zhou, A. G. Shen and J. M. Hu, *Chem. Commun.*, 2012, **48**, 3164–3166.
48 H. Zhou, J. Lee, T. J. Park, S. J. Lee, J. Y. Park and J. Lee, *Sens. Actuators, B*, 2012, **163**, 224–232.
49 H. Zhou, J. Kim, F. Zou, K. Koh, J. Y. Park and J. Lee, *Sens. Actuators, B*, 2014, **198**, 77–81.
50 X. Y. Li, Y. L. Zhou, Z. Z. Zheng, X. L. Yue, Z. F. Dai, S. Q. Liu and Z. Y. Tang, *Langmuir*, 2009, **25**, 6580–6586.
51 R. A. Reynolds, C. A. Mirkin and R. L. Letsinger, *J. Am. Chem. Soc.*, 2000, **122**, 3795–3796.
52 E. J. McCartney, *Optics of the Atmosphere: Scattering by Molecules and Particles*, John Wiley and Sons, Inc., New York, 1976, vol. 1, 421p.
53 J. Y. Song, C. H. Lee, E. J. Choi, K. Kim and J. Y. Yoon, *J. Virol. Methods*, 2011, **178**, 31–38.
54 K.-Y. Lien, J.-L. Lin, C.-Y. Liu, H.-Y. Lei and G. B. Lee, *Lab Chip*, 2007, **7**, 868–875.
55 J. R. Whiteaker, L. Zhao, H. Y. Zhang, L. C. Feng, B. D. Piening, L. Anderson and A. G. Paulovich, *Anal. Biochem.*, 2007, **362**, 44–54.
56 P. S. Mitchell, R. K. Parkin, E. M. Kroh, B. R. Fritz, S. K. Wyman, E. L. Pogosova-Agadjanyan, A. Peterson, J. Noteboom, K. C. O'Briant, A. Allen, D. W. Lin, N. Urban, C. W. Drescher, B. S. Knudsen, D. L. Stirewalt, R. Gentleman, R. L. Vessella, P. S. Nelson, D. B. Martin and M. Tewari, *Proc. Natl. Acad. Sci. U. S. A.*, 2008, **105**, 10513–10518.
57 W. J. Wiscombe, *Appl. Opt.*, 1980, **19**, 1505–1509.
58 A. Ashkin, J. M. Dziedzic, J. E. Bjorkholm and S. Chu, *Opt. Lett.*, 1986, **11**, 288–290.
59 M. D. Lecner, *J. Serb. Chem. Soc.*, 2005, **70**, 361–369.
60 M. Retsch, M. Schmelzeisen, H. J. Butt and E. L. Thomas, *Nano Lett.*, 2011, **11**, 1389–1394.
61 H. Xu, X. Chen, S. Ouyang, T. Kako and J. Ye, *J. Phys. Chem. C*, 2012, **116**, 3833–3839.
62 X. Liu, M. Atwater, J. Wang and Q. Huo, *Colloids Surf., B*, 2007, **58**, 3–7.